Altered morphology and 3D architecture of brain vasculature in a mouse model for Alzheimer's disease

Eric P. Meyer*, Alexandra Ulmann-Schuler*, Matthias Staufenbiel†, and Thomas Krucker‡§

*Department of Zoology, University of Zürich, Winterthurerstrasse 190, CH-8057 Zürich, Switzerland; ‡Novartis Institutes for BioMedical Research, Inc., Discovery Technologies, Cambridge, MA 02139; and †Novartis Institutes for BioMedical Research Basel, Nervous System Research, CH-4002 Basel, Switzerland

Edited by Floyd E. Bloom, The Scripps Research Institute, La Jolla, CA, and approved January 14, 2008 (received for review October 15, 2007)

Substantial evidence from epidemiological, pathological, and clinical reports suggests that vascular factors are critical in the pathogenesis of Alzheimer's disease (AD), and changes in blood flow are currently the most reliable indicators of the disease. We previously reported that older APP23 transgenic (tg) mice have significant blood flow alterations correlated with structural modifications of blood vessels. For the present study, our objective was to analyze the age-dependent morphological and architectural changes of the cerebral vasculature of APP23 tg mice. To visualize the 3D arrangement of the entire brain vasculature, we used vascular corrosion casts. Already at young ages, when typically parenchymal amyloid plaques are not yet present, APP23 tg mice had significant alterations, particularly of the microvasculature, often accompanied by small deposits attached to the vessels. In older animals, vasculature abruptly ended at amyloid plaques, resulting in holes. Often, small deposits were sitting near or at the end of truncated vessels. Between such holes, the surrounding vascular array appeared more dense and showed features typical for angiogenesis. We propose that small amyloid aggregates associated with the microvasculature lead to morphological and architectural alterations of the vasculature, resulting in altered local blood flow. The characteristic early onset of vascular alterations suggests that imaging blood flow and/or vasculature architecture could be used as a tool for early diagnosis of the disease and to monitor therapies.

amyloid precursor protein | cerebral blood flow | scanning electron microscopy | vascular corrosion casting

The typical clinical picture of Alzheimer's disease (AD) includes a progressive decline of memory function, often accompanied by other clinical signs such as agitation, aggression, sleep disturbances, and social withdrawal. Nonetheless, brain autopsy is needed to positively confirm the diagnosis (1). A high density of neuritic plaques, neurofibrillary tangles, and vascular amyloid (Aβ) is a characteristic neuropathological marker of AD (2, 3). Plaques and tangles in the neuropil may affect neuronal function and also contribute to the neuronal damage; however, it is unclear whether their incidence correlates with the clinical signs and symptoms of cognitive impairment characteristic of the disease (4). Evidence suggests that cerebrovascular pathologies, such as structural alterations (5), atherosclerotic lesions (6), and impaired hemodynamic responses (7), are early features of AD (for review, see ref. 8). Reduced blood flow has been reported as one of the most consistent physiological deficits in AD (9, 10); however, it remains unclear whether the reduced cerebral blood flow is a response to neuronal damage or a factor initiating the characteristic neuropathology. *In vivo* studies showed the effect of Aβ on cerebral blood flow and vessel architecture in a mouse model for AD (11, 12). In other models, cerebrovascular regulatory mechanisms, such as endothelium-dependent relaxation and cerebrovascular autoregulation, were altered before amyloid deposition (13–16). It also has been shown that Aβ *in vivo* and *in vitro* inhibits angiogenesis and at high dose can stimulate vascular degeneration (17), further strengthening the link between Aβ and the cerebrovascular abnormalities in AD. Moreover, risk factors for AD associated directly with vasculature include stroke, hypertension, diabetes, atherosclerosis, and hypercholesterolemia (18). These observations demonstrate the importance of studying vascular alterations during aging and amyloid formation.

Here, we describe the characteristic age-dependent alterations in cerebral vasculature of APP23 transgenic (tg) mice, which display typical pathological hallmarks of the disease, including neuritic plaques and amyloid deposition on blood vessels (19, 20). We produced vascular corrosion casts (VCC) from APP23 tg and littermate control mice of different ages (21), because unlike conventional histology, VCC retain the 3D architecture of the entire cerebral vasculature, including microvessels. SEM was used to image vessels at very high resolution suitable for studying the morphology of the vasculature. Based on our observations, we propose a model where minuscule amyloid deposits give rise to a local disturbance of the blood flow in capillaries, triggering a cascade of increased amyloid production/deposition resulting in vascular degeneration. Ultimately, holes are formed in the vascular system, accompanied by vascular remodeling. We show that holes likely are associated with larger amyloid plaques. Because of the characteristic and early onset of these vascular changes, imaging vascular alterations could be used as biomarker for the disease onset and progression and help to monitor AD therapies noninvasively.

Results

Cerebrovasculature in WT Animals. To describe the normal cerebral vascular morphology and architecture in mice we analyzed SEM images of 57 corrosion casts that were produced from 3- to 27-month-old APP23 WT littermate control mice (Fig. 1). Capillaries, the location of the blood–brain barrier, had diameters ranging from 4 to 6 μm. In WT animals, they formed a dense array often spaced <30 μm apart (Fig. 1*C*). On the cast surface of larger vessels, details of the endothelium, including imprints of endothelial nuclei and cell borders, enabled us to distinguish arteries from veins (22, 23). Typically in arteries, endothelial cells are elongated and aligned parallel with the long axis of the vessel, whereas those of veins are more rounded and less oriented (Fig. 1*D*). The details of the intricate features of normal cerebral vasculature using corrosion casts have been described by our group (21, 24, 25).

Vessel Eliminations Forming Holes Associated with Angiogenesis. To compare the vascular architecture of tg and WT mice, we

Author contributions: E.P.M. and A.U.-S. contributed equally to this work; E.P.M., A.U.-S., and T.K. designed research; E.P.M., A.U.-S., and T.K. performed research; E.P.M. and T.K. contributed new reagents/analytic tools; E.P.M., A.U.-S., and T.K. analyzed data; and E.P.M., A.U.-S., M.S., and T.K. wrote the paper.

The authors declare no conflict of interest.

This article is a PNAS Direct Submission.

Freely available online through the PNAS open access option.

§To whom correspondence should be addressed. E-mail: thomas.krucker@novartis.com.

This article contains supporting information online at www.pnas.org/cgi/content/full/0709788105/DC1.

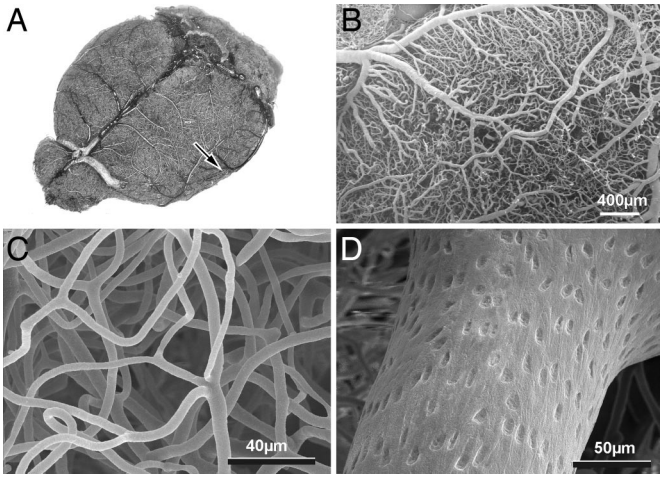

Fig. 1. Light micrograph and SEM images of VCCs from 4- to 8-month-old WT mice. (*A*) Stereomicroscopic image of the entire brain vasculature including the olfactory bulb. Clearly visible is the ascending middle cerebral artery (arrow) of the right cortical hemisphere and the veinal drainage at the surface. Cerebellum and pons (upper right-hand corner) are separated from the cortex by the transverse sinus. (*B*) Detail of the cortex illustrating the dense vascular network. (*C*) SEM image of cortical capillaries. Capillary diameters range from 4 to 6 μm and intercapillary distances are $\approx$30 μm. (*D*) Example of endothelial imprints on larger vessels. Here, the artery shows elongated cellular and nuclear imprints.

examined an additional 137 brains from APP23 tg mice. In APP23 tg mice, SEM pictures revealed holes in the dense network of the cortical vasculature, with dimensions varying from 0.03 to 3.5 mm^2 in older mice (Fig. 2). Within these holes, truncated microvessels were often studded with knobs and other abnormal protrusions (Fig. 2*C*). Additionally, holes occurred in correlation with vascular distortions, such as swelling and budding [Fig. 2*C* and supporting information (SI) Fig. 6]. Furthermore, the surrounding vasculature seemed much denser than in regions without apparent holes (Fig. 2*B*). Such vascular alterations are indicative of angiogenesis and typically appear in association with brain infarcts (26).

To analyze whether holes are located at sites of Aβ plaques, we visualized the plaque location with respect to the vasculature using 100-μm-thick sections of APP23 tg mouse brains, which were casted with PU4ii, but the tissue left intact. Thioflavin S-positive Aβ plaques were easily found in cortex and hippocampus by fluorescent light microscope (LM) (Fig. 2 *D–G*). We observed small and also large plaques (80–100 μm in diameter). Notably, parenchymal amyloid plaques were primarily situated in areas where vasculature was entirely absent, resembling the holes described above (Fig. 2 *D–G*). This finding supports the notion that holes observed in VCCs are the location of amyloid plaques.

Size and number of holes were examined in detail in at least four animals per age group (SI Table 1). We found that the mean number of holes per age group started to increase at 9 months of age in APP23 tg mice but seemed to plateau in older animals (Fig. 3*A*). A nonparametric Wilcoxon test showed a significant difference in the occurrence of holes between tg and WT mice ($P < 0.0001$), whereas the Kruskal–Wallis test revealed that the age effect is only borderline significant for tg ($P = 0.067$, $\chi^2 = 11.75$, df = 6) and not significant for WT animals ($P = 0.69$, $\chi^2 = 3.83$, df = 6). However, this finding is closely associated with the size of the holes.

To assess the affected area of the cerebral cortex (Fig. 3*B*), the mean hole size of each age group was multiplied by the number of holes. After a short lag-phase in younger mice, an exponential increase is observed in APP23 tg mice. Using a mixed model, a significant age effect is revealed for the hole size of tg mice ($P <$ 0.0001, numerator df = 6, denominator df = 61, F = 9.06). In WT animals, the holes affected only small areas of the cortex.

The position and the size of the holes are mapped on a simplified dorsal view of the mouse brain (Fig. 3*C*). This shows that the number and size of holes both increase with age. Holes prominently cluster in the frontal and temporal cortices.

With increased age and in parallel to the described holes, we observed that the vascular architecture in APP23 tg animals was considerably more disturbed than in aged WT animals. Microvessels showed several characteristic deformations like swelling, kinking, twisting, and looping, vascular abnormalities typical for AD and other dementias (27, 28).

Vessel Alterations, Pompons, and Cubes. Already in casts from 3-month-old APP23 tg mice, we found small knob-like structures of up to 14 μm in diameter attached to the vessels. In casts from

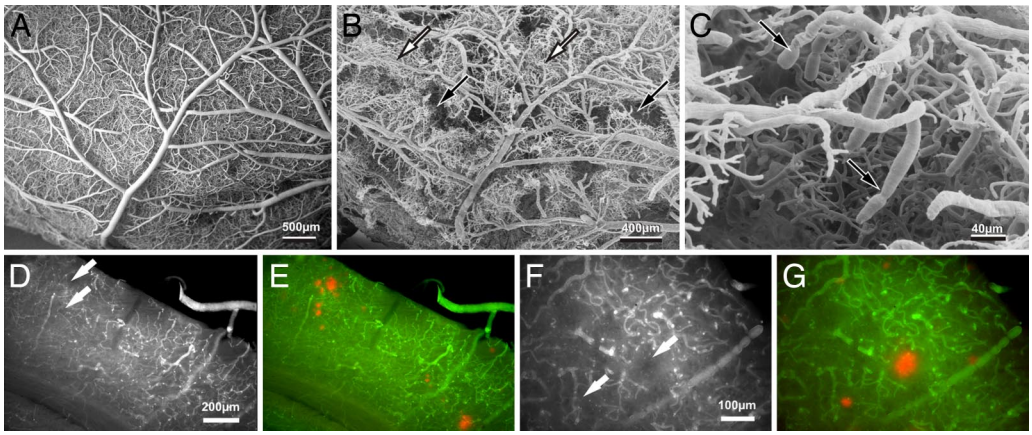

Fig. 2. Vessel deformation and elimination in older APP23 tg mice. (*A*) Overview of the left anterior cortex of a 18-month-old APP23 WT mouse. (*B*) In comparison, an 18-month-old APP23 tg mouse. The missing microvasculature is forming holes (black arrows) in the dense vascular network. Note that between the holes, the vasculature appeared much denser than in normal (WT) animals. (*C*) Detail of a hole illustrating the multitude of typical vessel deformations. Kinked and twisted microvessels can end abruptly and often have constrictions in the vicinity of the truncation (arrows). Other microvessels are studded and carry knob-like structures. (*D–G*) Thioflavin-S fluorescence labeled plaques in with PU casted brain tissue. Inherent fluorescence of PU allows visualizing the relation of the vasculature and plaques simultaneously. Tissue is from 18-month-old APP23 tg animals. Arrows in *D* and *F* point to holes associated with larger plaques in *E* and *G*.

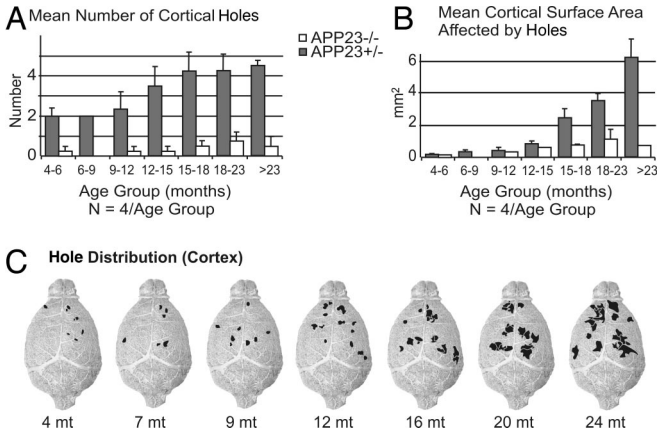

Fig. 3. Hole size, number, and distribution within cortical area of APP23 mice. (*A*) APP23 tg mice have already significant numbers of holes in the youngest age group (4–5), when typically other hallmarks of AD are absent. Interestingly, the mean number of holes plateaued after 15 months of age. However, the size of the holes (*B*) increased drastically in the APP23 tg mice at this age. Age-matched WT animals only occasionally had holes. (*C*) Holes were measured and mapped using SEM. Dark-colored patches delineate the spatial distribution and size of single holes at the cerebral cortex. With increasing age, hole size and number steadily increased. Hole distribution in APP23 tg mice appears clustered in patches in the frontal and temporal cortices.

4- to 5-month-old APP23 tg mice, these structures became more organized, showing protruding spikes (Fig. 4). They formed tufts attached to primarily small but also larger vessels. Because of their characteristic shape, we call these structures pompons. Most of the pompons were very small, the size varying between 8 and 15 μm in diameter. They followed a patchy distribution in CNS and in accordance with the expression pattern of mutated APP in these mice, pompons were occasionally also observed in the spinal cord. Single pompons could encircle capillaries and were colocalized with distorted microvessels (Fig. 4*B*). An additional type of structure attached to casted vessels showed a more cubical appearance and was composed of multiple flat or rough/jagged, sometimes rounded polygonal surfaces (Fig. 4*C*). These cubes were very similar in size to pompons. Interestingly, pompons and cubes could be colocalized on the same vessel. Occasionally, the same deposits displayed typical features of pompons and cubes combined. No similar structures were found in age-matched WT animals or in aged normal C57BL/6J or other mutant mice [e.g., IL6 or VEGF tg mice (29, 30)] that were processed in parallel for other studies. Thus, pompons and cubes were considered unique to APP tg mice.

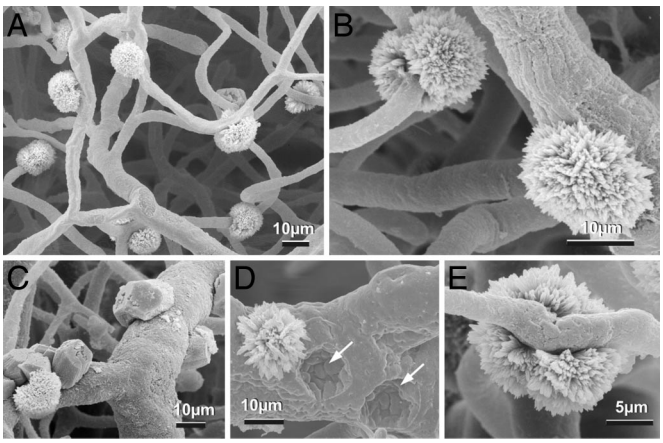

Fig. 4. Development of early vascular deposits (pompons and cubes) associated with microvasculature in 3- to 12-month-old APP23 tg mice. SEM images from whole-brain VCCs. (*A*) Accumulation of tuft-like structures with protruding spikes on microvessels. (*B–D*) Larger deposits are forming pompon-like structures that are between 8 and 15 μm in diameter. Pompons consist of fibrillar structures, can encircle and constrict capillaries (*B*), and are often associated with distortion of capillaries (*E*). (*C*) In older animals, structures of cubical appearance with multiple flat or rough and even rounded surfaces were found. Cubes are often colocalized with pompons. (*D*) Indentations resembling (white arrows) in size and shape imprints of detached pompons. Age of mice in *A*, *B* and *E*, 8.8 months; in *C*, 11.9 months; in *D*, 12 months.

The percentage of mice with deposits is shown in SI Fig. 7 and their location on the vascular tree in SI Table 2. In the investigated mice of different age groups (4–25 months), pompons and cubes were often found in young tg mice. In APP23 tg animals >14 months of age, the density of both structure types seemed to decrease. To investigate the sudden drop in frequency and eventual disappearance of the pompons and cubes in tg animals >15 months, we studied the casts from these age groups more closely. We observed small imprints in the cast surface neighboring pompons as illustrated in Fig. 4*D*. Imprints resembled negative impression of pompons, matched the diameter and shape of pompons and cubes and were more abundant in casts from older APP23 tg animals but never found in WT animals. For these old mice, our protocols required increased numbers and prolonged cycles of the maceration process using KOH and formic acid than typically used for casts from age-matched WT and young APP23 tg mice. We conclude that the absence of pompons and cubes in casts from older tg animals could be, at least partially, explained by our methods used to macerate and subsequently clean casts, which detached or dissolved pompons and cubes.

To further study the structure and chemical composition of the pompons and cubes, we cut thin histological sections of Epon-embedded Mercox casts. Microscopic analyses of both pompons and cubes revealed that their structure appeared different from the polymer forming the lumen of the vessels, which was more homogeneous. To test whether pompons or cubes might contain Aβ, we used immunohistochemical and classical amyloid staining procedures (SI Fig. 8). Thin sections of structures attached to vessel casts showed Thioflavin-S fluorescence, Congo red birefringence, and were stained by the polyclonal Aβ antibody NT11. Staining for the APP C terminus (antibody C8) was inconclusive (data not shown). These data suggested that pompons and cubes contain Aβ, which in contrast was never found in the vessel/resin portion of the casts. To support this finding, we isolated pompons and cubes from APP23 tg casts to test with MALDI MS. We found that Aβ fragments were the main constituents of these structures. No Aβ fragments were found in casting material isolated from WT mice (SI Table 3).

Discussion

The present study was conceived to elucidate the extent of deformations and eliminations that alter the morphology and architecture of the vasculature, particularly the microvasculature, in brains of APP23 tg mice. The combination of SEM and vascular corrosion casting is a powerful and unique method for studying vascular morphology and architecture. Our results show clearly that before amyloid plaques and other hallmarks of the disease appear, APP23 tg mice already have altered cerebrovasculature. Small structures in the shape of pompons and cubes that are positive for β-amyloid colocalize with architectural changes in the vasculature such as distortions. Because of their early appearance, these may represent initial lesions. At later stages, holes and increased microvascular density (Fig. 2) are dominant in cortical areas with high densities of amyloid plaques. Analysis of intact slices of casted brains further suggests that both microvascular alterations and holes are associated with larger parenchymal amyloid plaques. With respect to function, in

addition to our previous observations (11, 25), our new findings suggest that such morphological and architectural changes are correlated to disturbances in cerebral blood flow and may be linked to metabolic changes in AD brain.

Vascular Corrosion Casting, Vascular Morphology, and Network in WT Mice. It is remarkable that morphological and architectural alterations of vessels appear in APP23 tg mice at a very young age when typically none of the AD hallmarks in this model are detectable. We attribute this to the use of VCC, which allows the systematic study of the entire brain of a single mouse (24). The temporal and spatial development of AD hallmarks varies individually and the initial changes are small. Current technologies are limited to small samples from a single brain or lack the spatial resolution necessary to detect localized very small changes. However, besides the many advantages, such as exact 3D reproduction of the vascular architecture and vessels identifiable by characteristic pattern of endothelial cell imprints, the standard VCC technology combined with SEM suffers from several limitations. For this study, we have put special effort into improving this approach and developed methods that allow us to study the 3D vasculature in combination with the tissue. Using a combination of these methods with imaging technologies such as microCT (21, 24) will in future allow quantification of real 3D morphology and architecture.

Our present focus was on the cortical structures, and results show that the vascular network in normal and aged WT mice is highly organized and the capillary bed extremely dense with intervessel distances of ≈30 μm. Although we and others have shown that Mercox is shrinking substantially during curing (31, 32), we have additionally used a polyurethane that does not shrink (21). It has the added advantage over other currently available casting materials that it can be combined with immunohistochemical analysis of the surrounding tissue. Based on our measurements and visual analysis of the casted vascular network, we come to the conclusion that there is a tight spatial relationship between the vasculature and individual neurons (33). Therefore, it is evident that even small changes of blood flow in capillaries could have significant effects on neuronal metabolism and homeostasis.

Vessel Elimination and Angiogenesis: Hole Formation. In brains of older APP23 tg mice, we found missing vasculature, which manifested as visible holes in casts. Smaller holes were perfectly round. These holes are the sites of amyloid plaques as demonstrated with polyurethane casting combined with classical histological sectioning. Closer examination suggested that in many cases the vasculature immediately surrounding the hole was significantly denser. Detailed visual analysis also revealed the typical form and shape of truncated and deformed vasculature and signs of stenosis. However, the "budding" vasculature often interpreted as degenerating vasculature or not entirely perfused vessels as a possible technical artifact (22) was in the present case an indication of angiogenesis (26). In areas adjacent to the holes, the vasculature seemed to be denser than in corresponding areas of WT animals or normal vasculature within the same cast. Upon closer inspection of these areas, we found signs of angiogenesis (swelling, budding) as well. Although others have reported that in the immediate vicinity of amyloid plaques, vessel density is decreased (34), which may be because their analysis was restricted to 30 μm or thinner slices, there are recent findings that support the idea of increased angiogenic activity immediately around amyloid accumulations. In an elegant study, Yang *et al.* (35) have shown colocalization of amyloid plaques with significantly increased accumulation of vascular endothelial growth factor (VEGF) in tissue from AD patients. Similar findings were recently reported for APP23 mice (36). Activation of endothelium was significantly increased with age of the APP23 tg mice and β3-integrin expression, a specific marker for activated endothelium, restricted to amyloid positive vessels. Moreover, homogenates from APP23 tg mice induced the formation of new vessels in an *in vivo* angiogenesis assay. Studies in a cerebral ischemia model clearly showed a strong increase in the number of newly formed vessels at the border of infarcts within 2–3 days (37). Microglial cells like macrophages associating with the injured area may additionally contribute to angiogenesis in AD brain, because they abundantly express VEGF (38, 39). In fact, Perry's group has reported higher capillary density in the zone directly surrounding amyloid plaques in tissue from AD subjects (40).

In APP23 tg mice, we observed a strong correlation of the number of holes with increasing age and pathological progression of the disease. This augmentation seemed to plateau at 15 months of age. This seems because, in older mice, several smaller neighboring holes combine into one larger hole. In contrast, only very few and small holes were found in control animals. These findings suggest that holes are very rare during normal aging but are dramatically increased by amyloid deposition. Furthermore, examinations in AD patients have shown that brain infarction plays an important role in determining the presence and the severity of AD symptoms (41, 42). However, Roher *et al.* have shown that such infarction in AD is closely related to atherosclerotic processes (6).

Pompons and Cubes: Early Amyloid Deposition. We found small knob-like structures on the casted vasculature, most pronounced on microvessels like capillaries at a time point when neither parenchymal nor vascular amyloid deposits were present (20, 43, 44). They could form two different structures, which we described as pompons and cubes, both extruding into endothelial cells and/or neuropil and staining positive for amyloid. 2D analyses of vascular deposits in older APP23 tg mice show striking similarities in location and shape to pompons (19). Interestingly, similar vessels associated amyloid structures were observed in tissue from AD subjects. Notably, Kawai *et al.* (40) reported that between 60% and 77% of amyloid plaques smaller than 35 μm in diameter were associated with capillaries. In an EM study, Miyakawa *et al.* (45) described that capillaries usually run through plaques or the boundary, and amyloid fibrils occur in the basement membrane, extended radially into the parenchyma and also into endothelial cells. Often the lumen of the vessels were narrowed and occluded. The earlier occurrence and smaller size suggest that pompons may be starting points of amyloid deposition. Roher *et al.* (46), analyzing Aβ species of cerebrovascular amyloid, described structures that seem to be analogues to pompons (46). In addition, their findings support our MALDI data that these structures contain Aβ 1–42. Because Aβ in APP23 tg mice is of neuronal origin and present at high concentrations throughout the brain also in young mice (47), we suggest that during a removal process, Aβ is transported to the vasculature and may accumulate in or around endothelial cells (9, 48, 49). Our model describing the interplay between amyloid and the vasculature leading to the observed vascular alterations is described in Fig. 5. Furthermore, in both young and old APP23 tg mice, we visualized distorted blood vessels comparable to vascular abnormalities found at autopsy in brains of AD subjects.

Conclusion

Because vascular alterations appear in young APP23 tg mice before pathological hallmarks of AD develop (8), our observation supports the idea that a disrupted microvasculature integrity could contribute to the course of events leading to the disease. These vascular changes may also be responsible for the early behavioral changes in young APP23 tg mice manifested as learning and memory deficits (50, 51). Cerebral microcirculatory

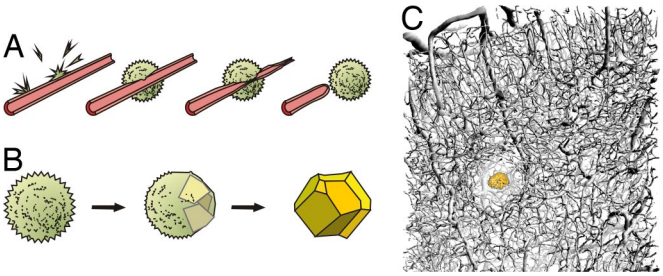

Fig. 5. Model of deposit and hole formation. (*A*) Aβ of neuronal origin pursuing a drainage pathway gradually accumulates at small blood vessels. After forming a core, which facilitates deposition, new Aβ fibrils adhere and subsequently form larger deposits in the form of pompons. (*B*) At a later stage, pompons can form cubes through additional Aβ or other protein depositions and transform into larger aggregates such as vascular amyloid deposits. Our model suggests that both structures can cause vessel elimination through stenosis (perhaps by inducing a coagulative necrosis downstream) or through a direct toxic effect of Aβ initiating vessel degeneration (17). Vessel deformations may include single or repeated constrictions along a vessel with direct effects on haemodynamics that ultimately result in vessel irregularities, vessel elimination, and also the formation of holes in the tight network of the vasculature (also see Figs. 3, and 4). (*C*) Artistic rendering of a hole with amyloid plaque. The model suggests that holes form around larger amyloid deposits and could therefore be used as biomarkers for brain damage in AD.

impairment evolving slowly and progressively over many years could be a causal factor of AD pathogenesis and may be other forms of dementia. Imaging vasculature could therefore be used for early diagnosis of the disease and as an efficient tool to monitor therapies.

Materials and Methods

Animals. The generation of APP23 tg mice is described in detail elsewhere (20). Briefly, a murine Thy-1 promoter element was used to drive neuron-specific expression of a human mutated APP751 (Swedish double mutation KM670/671NL) cDNA in B6D2 mice. The mice have been backcrossed with C57BL/6J mice for >10 generations. A total of 80 heterozygous tg and 57 WT littermate control male and female APP23 mice, ranging from 3 to 27 months of age, have been used for this study. All animal experimental procedures were carried out in compliance with National Institutes of Health Guidelines for Care and Use of Laboratory Animals.

VCCs. Mice were deeply anesthetized with 100 mg/kg pentobarbital (i.p.) and perfused through the left ventricle, first with ACSF containing Heparin (52) followed by 4% performaldehyde in PBS, followed by the resin Mercox (Ladd Research), both infused at the same rate. Afterwards, resin curing soft tissue was macerated followed by decalcification with 5% formic acid (53). Casts were washed, then dried by lyophilization, mounted on stubs, and sputter-coated with gold for routine SEM.

Selected animals were perfused with a new polyurethane resin PU4ii (vasQtec) instead of Mercox. The characteristics of this casting material are described in detail elsewhere (21). PU4ii is fluorescent and, because of its physical characteristics, suited for standard histological analysis. With this protocol, soft tissue combined with the cast was analyzed. (see also *SI Methods*)

Histology, Immunohistochemistry, and MALDI MS. To assess chemical composition of vascular deposits (pompons and cubes; see below), single branches from Mercox casts were embedded in Epon 812 and cut in 1-μm sections with an ultramicrotome. Paraffin sections (5 μm) from conventionally fixed animals were used as controls. Congo red and Thioflavin-S staining were done according to standard protocols (54). The following antibodies were used: polyclonal antibody to Aβ (NT11) (20), polyclonal antibodies to APP (C8) (19), and, as a secondary antibody, CY3 (Jackson Immunoresearch).

For simultaneous analysis of Aβ plaques and vasculature, brains were casted with PU4ii, and tissue kept intact. One hundred-micrometer sections were made with a Vibratome (Campden Instruments). The slices then were stained for amyloid deposits with 1% Thioflavin S solution (55). The embedded slices were observed in a fluorescent LM and in a confocal laser scanning microscope (Leica Microsystems).

In addition, isolated deposits (pompons) and casting material were analyzed with MALDI MS using a commercial instrument with modifications as described in Stoeckli *et al.* (56).

Quantification and Statistics. To establish a temporal distribution of the vascular alterations, the investigated corrosion casts were divided into seven age groups (0- to 6-, 6- to 9-, 9- to 12-, 12- to 15-, 15- to 18-, 18- to 23-, and >23-month-old animals). We focused on the analysis of the cerebral cortex to address the described high plaque load in the neocortex and hippocampus in APP23 tg mice (57).

For the quantification of pompons and cubes, 5–15 animals per age group were examined, with the exception of >23-month-old control mice, where only three casts were available. The age dependence of vascular deposits was tested with a linear model for discrete data. A one-tailed Student's *t* test was performed by using the software S-Plus (Insightful Corporation). The results were considered significant at $P = 0.05$ for a $t \geq 1.7$.

In APP23 tg and WT mice ($n = 4$), hole quantifications of SEM pictures were performed in different age groups. In both hemispheres of the cortex, holes that fulfilled the stated criteria were counted. Criteria were compiled around the holes, such as microvascular deposits (pompons or cubes), twisted or kinked vessels, and other microvascular alterations (27, 58). Afterward, all hole areas were measured and processed with the imaging software Image-Pro Plus (Media Cybernetics), by outlining the holes in the vasculature. The evaluation of age-dependent changes in number, size, and position of holes was performed by visually interpreting diagrams and a protocol, where the hole distribution pattern of four mice per age group was plotted.

To analyze the effect of age on size of holes, a mixed model was performed (SAS/STAT Software, 1999). The parameter ''mouse'' was assessed as random effect, because several measurements were done for each animal. To check the effect of age on the number of holes, nonparametric tests were performed separately for each genotype (one-sided Wilcoxon two-sample test and Kruskal–Wallis for more than two samples). The results of these tests were considered significant at $P \leq 0.05$.

ACKNOWLEDGMENTS. We thank Stefan Heinzer for help with the 3D reconstruction of vasculature, Axel Lang for expert advice on polyurethanes, and Jerome Frei for help with the MALDI experiments. E.P.M. and A.U.-S. were supported by a grant from Novartis.

1. McKhann G, *et al.* (1984) Clinical diagnosis of Alzheimer's disease: Report of the NINCDS-ADRDA Work Group under the auspices of Department of Health and Human Services Task Force on Alzheimer's Disease. *Neurology* 34:939–944.
2. Probst A, Langui D, Ulrich J (1991) Alzheimer's disease: A description of the structural lesions. *Brain Pathol* 1:229–239.
3. Terry RD KR, Bick KL, Sisodia SS (1994) *Alzheimer Disease* (Raven, New York).
4. Prohovnik I, *et al.* (2006) Dissociation of neuropathology from severity of dementia in late-onset Alzheimer disease. *Neurology* 66:49–55.
5. Shi J, Perry G, Smith MA, Friedland RP (2000) Vascular abnormalities: the insidious pathogenesis of Alzheimer's disease. *Neurobiol Aging* 21:357–361.
6. Roher AE, Esh C, Rahman A, Kokjohn TA, Beach TG (2004) Atherosclerosis of cerebral arteries in Alzheimer disease. *Stroke* 35:2623–2627.
7. Johnson KA, Albert MS (2000) Perfusion abnormalities in prodromal AD. *Neurobiol Aging* 21:289–292.
8. Iadecola C (2004) Neurovascular regulation in the normal brain and in Alzheimer's disease. *Nat Rev Neurosci* 5:347–360.
9. Bateman GA, Levi CR, Schofield P, Wang Y, Lovett EC (2006) Quantitative measurement of cerebral haemodynamics in early vascular dementia and Alzheimer's disease. *J Clin Neurosci* 13:563–568.
10. de la Torre JC, Mussivand T (1993) Can disturbed brain microcirculation cause Alzheimer's disease? *Neurol Res* 15:146–153.
11. Beckmann N, *et al.* (2003) Age-dependent cerebrovascular abnormalities and blood flow disturbances in APP23 mice modeling Alzheimer's disease. *J Neurosci* 23:8453–8459.
12. Mueggler T, *et al.* (2002) Compromised hemodynamic response in amyloid precursor protein transgenic mice. *J Neurosci* 22:7218–7224.
13. Iadecola C, *et al.* (1999) SOD1 rescues cerebral endothelial dysfunction in mice overexpressing amyloid precursor protein. *Nat Neurosci* 2:157–161.
14. Niwa K, *et al.* (2000) A beta 1–40-related reduction in functional hyperemia in mouse neocortex during somatosensory activation. *Proc Natl Acad Sci USA* 97:9735–9740.
15. Niwa K, *et al.* (2002) Cerebrovascular autoregulation is profoundly impaired in mice overexpressing amyloid precursor protein. *Am J Physiol* 283:H315–H323.
16. Wu Z, *et al.* (2005) Role of the MEOX2 homeobox gene in neurovascular dysfunction in Alzheimer disease. *Nat Med* 11:959–965.
17. Paris D, *et al.* (2004) Inhibition of angiogenesis by Abeta peptides. *Angiogenesis* 7:75–85.
18. de la Torre JC (2004) Is Alzheimer's disease a neurodegenerative or a vascular disorder? Data, dogma, and dialectics. *Lancet Neurol* 3:184–190.

19. Calhoun ME, *et al.* (1999) Neuronal overexpression of mutant amyloid precursor protein results in prominent deposition of cerebrovascular amyloid. *Proc Natl Acad Sci USA* 96:14088–14093.
20. Sturchler-Pierrat C, *et al.* (1997) Two amyloid precursor protein transgenic mouse models with Alzheimer disease-like pathology. *Proc Natl Acad Sci USA* 94:13287–13292.
21. Krucker T, Lang A, Meyer EP (2006) New polyurethane-based material for vascular corrosion casting with improved physical and imaging characteristics. *Microsc Res Technol* 69:138–147.
22. Christofferson RH, Nilsson BO (1988) Microvascular corrosion casting with analysis in the scanning electron microscope. *Scanning* 10:43–63.
23. Miodonski AJ, Hodde KC, Bakker C (1976) Scanning electron microscopy of plastic corrosion casts: The morphological distinction of arteries and veins. *Beitr Elektronmikroskop Direktabb Oberfl*, 435–442.
24. Heinzer S, *et al.* (2006) Hierarchical microimaging for multiscale analysis of large vascular networks. *NeuroImage* 32:626–636.
25. Krucker T, Schuler A, Meyer EP, Staufenbiel M, Beckmann N (2004) Magnetic resonance angiography and vascular corrosion casting as tools in biomedical research: application to transgenic mice modeling Alzheimer's disease. *Neurol Res* 26:507–516.
26. Liu HM (1988) Neovasculature and blood-brain barrier in ischemic brain infarct. *Acta Neuropathol (Berl)* 75:422–426.
27. Hassler O (1967) Arterial deformities in senile brains. The occurrence of the deformities in a large autopsy series and some aspects of their functional significance. *Acta Neuropathol (Berl)* 8:219–229.
28. Zarow C, Barron E, Chui HC, Perlmutter LS (1997) Vascular basement membrane pathology and Alzheimer's disease. *Ann NY Acad Sci* 826:147–160.
29. Campbell IL (1998) Transgenic mice and cytokine actions in the brain: bridging the gap between structural and functional neuropathology. *Brain Res Rev* 26:327–336.
30. Heinzer S, *et al.* (2007) Novel three-dimensional analysis tool for vascular trees indicates complete micro-networks, not single capillaries, as the angiogenic endpoint in mice overexpressing human VEGF(165) in the brain. *NeuroImage* 39:1549–1558.
31. Lametschwandtner A, Lametschwandtner U, Weiger T (1990) Scanning electron microscopy of vascular corrosion casts-technique and applications: updated review. *Scan Microsc* 4:889–940.
32. Weiger T, Lametschwandtner A, Stockmayer P (1986) Technical parameters of plastics (Mercox CL-2B and various methylmethacrylates) used in scanning electron microscopy of vascular corrosion casts. *Scan Electron Microsc* 243–252.
33. Abbott NJ, Ronnback L, Hansson E (2006) Astrocyte-endothelial interactions at the blood-brain barrier. *Nat Rev Neurosci* 7:41–53.
34. Kouznetsova E, *et al.* (2006) Developmental and amyloid plaque-related changes in cerebral cortical capillaries in transgenic Tg2576 Alzheimer mice. *Int J Dev Neurosci* 24:187–193.
35. Yang SP, *et al.* (2004) Coaccumulation of vascular endothelial growth factor with beta-amyloid in the brain of patients with Alzheimer's disease. *Neurobiol Aging* 25:283–290.
36. Schultheiss C, *et al.* (2006) *In vivo* characterization of endothelial cell activation in a transgenic mouse model of Alzheimer's disease. *Angiogenesis* 9:59–65.
37. Marti HJ, *et al.* (2000) Hypoxia-induced vascular endothelial growth factor expression precedes neovascularization after cerebral ischemia. *Am J Pathol* 156:965–976.
38. Carmeliet P, Storkebaum E (2002) Vascular and neuronal effects of VEGF in the nervous system: implications for neurological disorders. *Semin Cell Dev Biol* 13:39–53.
39. Kovacs Z, Ikezaki K, Samoto K, Inamura T, Fukui M (1996) VEGF and flt. Expression time kinetics in rat brain infarct. *Stroke* 27:1865–1872; discussion 1872–1863.
40. Kawai M, Kalaria RN, Harik SI, Perry G (1990) The relationship of amyloid plaques to cerebral capillaries in Alzheimer's disease. *Am J Pathol* 137:1435–1446.
41. Snowdon DA, *et al.* (1997) Brain infarction and the clinical expression of Alzheimer disease. The Nun Study. *J Am Med Assoc* 277:813–817.
42. Wright CB, Vonsattel JP, Bell K, Honig LS (2006) Dementia with cerebrovascular disease. *Sci Aging Knowledge Environ*, PMID 16807476.
43. Winkler DT, *et al.* (2001) Spontaneous hemorrhagic stroke in a mouse model of cerebral amyloid angiopathy. *J Neurosci* 21:1619–1627.
44. Burbach GJ, *et al.* (2007) Vessel ultrastructure in APP23 transgenic mice after passive anti-Abeta immunotherapy and subsequent intracerebral hemorrhage. *Neurobiol Aging* 28:202–212.
45. Miyakawa T, Sumiyoshi S, Murayama E, Deshimaru M (1974) Ultrastructure of capillary plaque-like degeneration in senile dementia. Mechanism of amyloid production. *Acta Neuropathol* 29:229–236.
46. Roher AE, *et al.* (1993) Beta-Amyloid-(1–42) is a major component of cerebrovascular amyloid deposits: implications for the pathology of Alzheimer disease. *Proc Natl Acad Sci USA* 90:10836–10840.
47. Kuo YM, *et al.* (2001) Comparative analysis of amyloid-beta chemical structure and amyloid plaque morphology of transgenic mouse and Alzheimer's disease brains. *J Biol Chem* 276:12991–12998.
48. Ji Y, Permanne B, Sigurdsson EM, Holtzman DM, Wisniewski T (2001) Amyloid beta40/42 clearance across the blood-brain barrier following intraventricular injections in wild-type, apoE knockout and human apoE3 or E4 expressing transgenic mice. *J Alzheimers Dis* 3:23–30.
49. Zlokovic BV (2004) Clearing amyloid through the blood-brain barrier. *J Neurochem* 89:807–811.
50. Van Dam D, *et al.* (2003) Age-dependent cognitive decline in the APP23 model precedes amyloid deposition. *Eur J Neurosci* 17:388–396.
51. Prut L, *et al.* (2007) Aged APP23 mice show a delay in switching to the use of a strategy in the Barnes maze. *Behav Brain Res* 179:107–110.
52. Krucker T, Siggins GR, Halpain S (2000) Dynamic actin filaments are required for stable long-term potentiation (LTP) in area CA1 of the hippocampus. *Proc Natl Acad Sci USA* 97:6856–6861.
53. Meyer EP (1989) Corrosion casts as a method for investigation of the insect tracheal system. *Cell Tissue Res* 256:1–6.
54. Ravens JR (1978), in *Three dimensional microanatomy of cells and tissue surfaces*, Cervos-Navarro J, ed (Raven, New York), pp 487–501.
55. Tong XK, Nicolakakis N, Kocharyan A, Hamel E (2005) Vascular remodeling versus amyloid beta-induced oxidative stress in the cerebrovascular dysfunctions associated with Alzheimer's disease. *J Neurosci* 25:11165–11174.
56. Stoeckli M, Staab D, Staufenbiel M, Wiederhold KH, Signor L (2002) Molecular imaging of amyloid beta peptides in mouse brain sections using mass spectrometry. *Anal Biochem* 311:33–39.
57. Sturchler-Pierrat C, Staufenbiel M (2000) Pathogenic mechanisms of Alzheimer's disease analyzed in the APP23 transgenic mouse model. *Ann NY Acad Sci* 920:134–139.
58. Beskow J, Hassler O, Ottosson JO (1971) Cerebral arterial deformities in relation to senile deterioration. *Acta Psychiatr Scand Suppl* 221:111–119.